Experimental Mechanics (2007) 47: 51–62
DOI 10.1007/s11340-006-0531-2

Micro- and Nanoscale Deformation Measurement of Surface and Internal Planes via Digital Image Correlation

T.A. Berfield · J.K. Patel · R.G. Shimmin · P.V. Braun · J. Lambros · N.R. Sottos

Received: 30 March 2006 / Accepted: 11 October 2006 / Published online: 11 January 2007

Abstract The digital image correlation (DIC) technique is successfully applied across multiple length scales through the generation of a suitable speckle pattern at each size scale. For microscale measurements, a random speckle pattern of paint is created with a fine point airbrush. Nanoscale displacement resolution is achieved with a speckle pattern formed by solution deposition of fluorescent silica nanoparticles. When excited, the particles fluoresce and form a speckle pattern that can be imaged with an optical microscope. Displacements are measured on the surface and on an interior plane of transparent polymer samples with the different speckle patterns. Rigid body translation calibrations and uniaxial tension experiments establish a surface displacement resolution of 1 μm over a 5×6 mm scale field of view for the airbrushed samples and 17 nm over a 100×100 μm scale field of view for samples with the fluorescent nanoparticle speckle. To demonstrate the capabilities of the method, we characterize the internal deformation fields generated around silica microspheres embedded in an elastomer under tensile loading. The DIC technique enables measurement of complex deformation fields with nanoscale precision over relatively large areas, making it of particular relevance to materials that possess multiple length scales.

Keywords Digital image correlation · Nanoparticle · Displacement measurement · Multiscale · Deformation

T.A. Berfield (✉, SEM member) · J.K. Patel · R.G. Shimmin · P.V. Braun · J. Lambros (SEM member) · N.R. Sottos (SEM member)
University of Illinois at Urbana–Champaign, Urbana, IL, USA
e-mail: berfield@uiuc.edu

Introduction

Many materials possess a hierarchical structure that spans several length scales. While bulk properties and performance can be obtained through macroscale testing and characterization, many processes occurring at the microscale and nanoscale cannot be fully understood based solely on macroscale testing. Fracture mechanisms, for example, must be analyzed by separating the relative importance of microstructural and nanostructural hierarchy effects on critical events such as crack initiation, subsequent propagation and consequent unstable fracture [1]. Testing methods are required that can achieve measurement resolutions on the order of microns and nanometers, and can be implemented over a range of length scales. Localized measurements, such as micro- or nanoindentation, provide limited data that are often difficult to extend to larger length scales. Other high resolution imaging techniques, such as Atomic Force or Scanning Tunneling Microscopy (AFM/STM) and Near Field Scanning Optical Microscopy (NFSOM), are full-field but involve bringing a tip on or very near the surface and thus are not entirely suitable for use with soft (e.g., biological) materials. In addition, these are rastering techniques and limited in real-time visualization capability as well as the size of the rastered area. Electron microscopy techniques such as STEM (Scanning/Transmission Electron Microscopy) and micro-Computed Tomography (μCT) have similar drawbacks, but can provide internal information.

Digital Image Correlation (DIC) is a robust experimental method enabling full-field real-time measurements, either on the surface or in the interior (for transparent media) of a deforming body. Digital image

correlation is a computer-based process to obtain two dimensional full-field displacement information by recording the motion of a speckle pattern on a specimen surface (Fig. 1) before and after deformation [2–5]. Assuming a locally homogeneous deformation over a small subset of the specimen, the deformed coordinates (x_q', y_q') of a material point q in the neighborhood of a point p, at undeformed location (x_p, y_p), are given by

$$x'_q = x_q + u_p + \frac{\partial u_p}{\partial_x}\Delta x_q + \frac{\partial u_p}{\partial_y}\Delta y_q,$$
$$y'_q = y_q + v_p + \frac{\partial v_p}{\partial_y}\Delta y_q + \frac{\partial v_p}{\partial_x}\Delta x_q, \quad (1)$$

where u_p and v_p are the x and y components of the displacement vector of point p, respectively, x_q and y_q are the undeformed coordinates of point q, $\Delta x_q = x_q - x_p$ and $\Delta y_q = y_q - y_p$.

The displacement of a point p is found by either minimizing a least-square correlation coefficient, or maximizing a cross-correlation coefficient, of the grayscale intensity value before and after deformation, over a small locally homogeneous square subset S centered around p [4]. Since the grayscale intensity of a point is assumed to be invariant with deformation, the correlation depends on the original position of point p and the parameters describing its deformation, i.e., vector $\overrightarrow{V} = \left(u, v, \frac{\partial u}{\partial x}, \frac{\partial v}{\partial y}, \frac{\partial u}{\partial y}, \text{and} \frac{\partial v}{\partial x}\right)$, the unknown deformation. Changes introduced to the grayscale intensity of the pattern, such as fluctuations of the light source, will affect the accuracy of the correlation. During the minimization process to find the unknown vector $\overrightarrow{V}$, interpolation between pixels produces subpixel accuracy in the correlated displacement field of about one-tenth of a pixel [6]. The interpolation errors associated with the correlation minimization scheme will also influence the measurement accuracy.

DIC is an attractive technique for use over multiple length scales since the method does not possess an inherent length scale. The accuracy of the correlation between recorded images depends upon the quality of the image speckle pattern and the resolution of the imaging system. Physical units of displacement are obtained by multiplying the pixel-based measurements of DIC by the image resolution in pixels/unit length. The ability to perform digital image correlations on a particular pattern is highly dependent on the refinement, distribution, and randomness of the speckle relative to the pixel size in the image, as well as the dimensions of the subset used in the correlation. While there are no well-defined guidelines on the optimization of the imaged speckle size relative to the pixel size, a pattern can be qualitatively described by the image intensity profile, where the number of pixels at a given grayscale intensity value ranging from 0 to 255 is plotted against that intensity value. Unacceptable

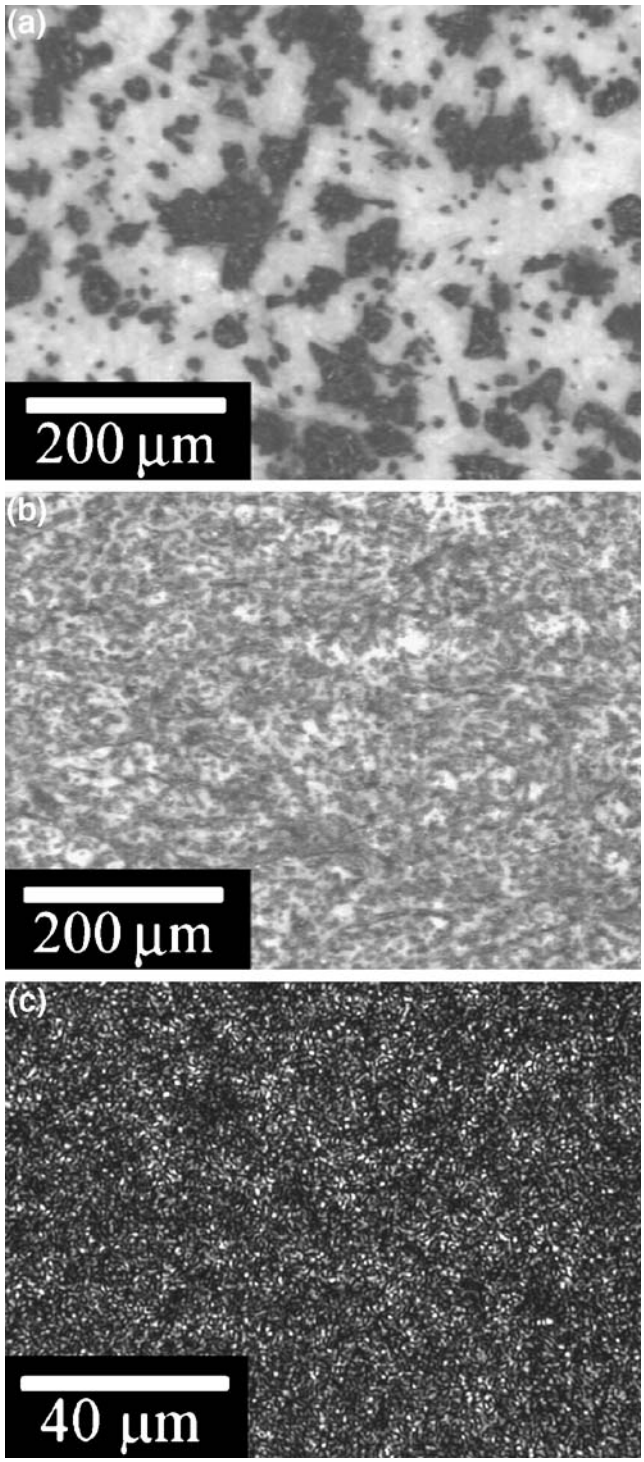

Fig. 1 Speckle patterns tailored for the specific magnification required. (**a**) A pattern created by a low-quality airbrush (Badger 250), (**b**) a pattern created by a higher-quality airbrush (Iwata Custom Micron B) and (**c**) a pattern created by fluorescent nanoparticle surface deposition are shown at similar magnifications

patterns, i.e. ones that will not correlate with accurate results, produce a bimodal distribution, Fig. 2(a), with dominant peaks at either end of the grayscale spectrum [7]. Patterns more appropriate to image correlation have been observed to possess either a Gaussian or bell-shaped distribution, Fig. 2(b) and (c).

DIC has been successfully coupled with optical microscopy in the past to obtain full-field surface displacement measurements with microscale accuracy. Gonzalez and Knauss [8] proved the feasibility of the technique and Abanto-Bueno and Lambros [9] extended the method to real-time measurements while imaging craze development in polyethylene. Digital image correlation is also suitable for nanoscale measurements when coupled with imaging techniques such as STM and AFM. Vendroux et al. [10] used DIC with an STM to investigate the fiber/matrix interphase response in polymer matrix composites. Chasiotis and Knauss [6] successfully combined DIC with AFM imaging to measure the elastic properties of polysilicon. The AFM/DIC set-up of Chasiotis and Knauss [6] had a resolution of ca. 5 nm displacement, over a 10 μm field of view. However, unlike microscale DIC experiments where paint was used to obtain a surface speckle pattern, in the nanoscale studies the speckle pattern is dependent on the surface roughness profile of the sample material.

In this paper, we discuss the application of DIC for full-field real-time measurements both at the micro- and the nanoscale, performed on either the patterned surface or an interior plane (for transparent media) of a deforming body. An optical microscope is used as the imaging device, thus considerably simplifying the experimental set-up over that requiring an AFM/STM. An important aspect of this work is the generation of a suitable speckle pattern for use with DIC at each size scale (Fig. 1). The same DIC correlation algorithm is used with macro-, micro- or nanoscale resolution if the specimen surface coating technique is modified such that a correlatable pattern is obtained in each case. Lower resolution DIC measurements employ a simple method such as spray painting to generate a surface pattern for DIC at image resolutions only as low as 10 μm/pixel [9, 11]. Figure 1(a) shows a magnified view of a pattern that is unsuitable for DIC at the scale shown. For the microscale experiments in the current work, a fine point airbrush is used to generate a speckle pattern [Fig. 1(b)], while for nanoscale experiments fluorescent nanoparticle tracers are employed [Fig. 1(c)] [12]. Rigid body translation and uniaxial tension experiments are carried out separately to establish the displacement resolutions at each scale. For this work, the scope of the experiments is limited to small strains in isotropic elastomers.

Specimen Preparation

Transparent polymer samples were prepared with DIC patterns at two different size scales for displacement measurements on the surface [Fig. 3(a)] and on an internal plane [Fig. 3(b)]. Table 1 summarizes the details of sample preparation, the patterning technique and image acquisition for each sample type as described below.

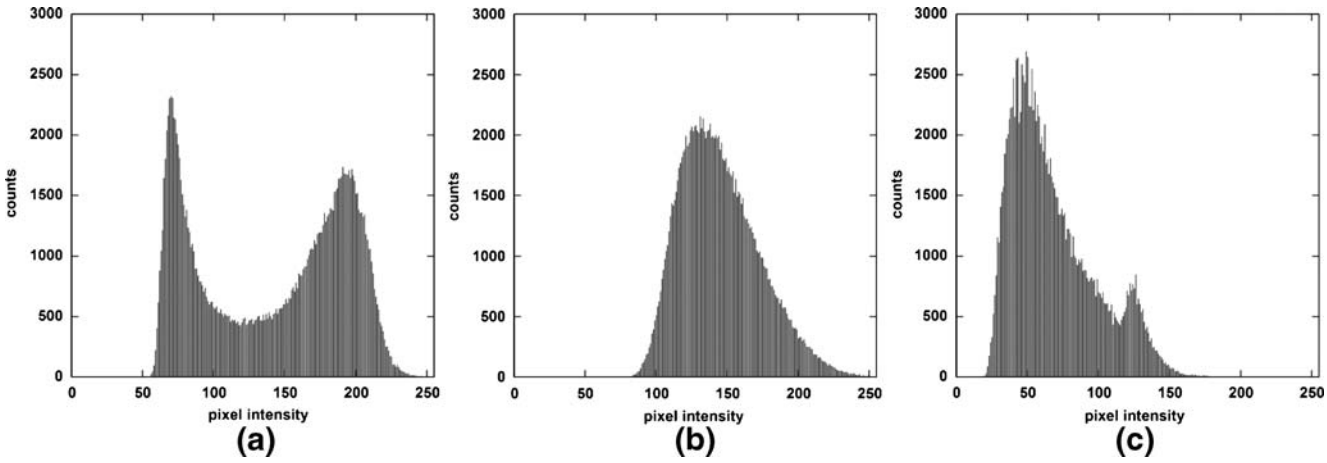

Fig. 2 Pixel intensity histograms for the patterns presented in Fig. 1: (**a**) coarse paint pattern made with the Badger airbrush which provides poor correlations, and acceptable DIC patterns created using (**b**) an Iwata fine-nozzle airbrush, and (**c**) the deposition of nanoparticles

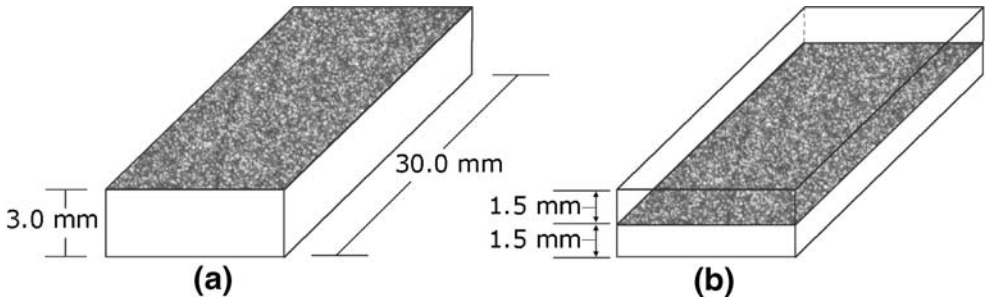

Fig. 3 Schematic representation of (**a**) surface patterned, and (**b**) internally patterned samples prepared for digital image correlation

Microscale Airbrush DIC Pattern

Surface pattern

Following the method outlined in Patel, [13] speckle patterns suitable for DIC at image resolutions ranging from 3 to 10 μm/pixel were applied to sheets of a polyethylene–carbon monoxide (ECO) copolymer (ITW-HiCone, Inc.) using an Iwata Custom Micron B airbrush. The nozzle diameter of this airbrush is 0.18 mm which allows for greater paint diffusion resulting in smaller paint droplets (speckles) than those in Abanto-Bueno and Lambros [9, 11]. In addition, its gravity-feed system when coupled with a lighter weight drawing ink provided excellent consistency. Air was provided by a constant 100 psi pressure regulated compressed air system. When viewed under a microscope as shown in Fig. 1(b), the new pattern produces an image with similar characteristics to images previously known to have worked with DIC.

Internal pattern

For internal measurements, a transparent silicone rubber (GE Silicones, RTV-615) was chosen to enable optical imaging through the thickness of the sample. Specimens were prepared through a two step process. Initially, one polymer layer was cast into a multipart mold to a thickness of approximately 1.5 mm and allowed to cure partially at room temperature for 24 h. While the exposed surface was still tacky because of partial curing, a speckle pattern was sprayed on it using the method described above. After allowing the ink to dry for a few minutes, a second layer of silicone rubber, also 1.5 mm thick, was poured onto the first. The entire casting was then left for a few days to cure completely, after which time the specimens were removed from the mold and cut to final dimensions. The resulting internal speckle pattern was similar to the surface one shown in Fig. 1(b).

A second set of microscale airbrush patterned samples were made in a similar manner, with the additional step of adding a dilute concentration of silica glass microspheres (with radii $r = 70 - 80\ \mu$m) on top of the patterned bottom layer. After deposition of the top layer, the resulting specimen had internally embedded spheres with a patterned plane located just below it at $z=-r$ (for $z=0$ at the sphere midplane). The patterned layer and embedded microspheres were situated the same as with the other samples, halfway through the sample thickness [Fig. 3(b)]. Polydimethylsiloxane (PDMS) was substituted as the matrix material in this case for meaningful comparisons with nanoparticle patterned samples.

Table 1 Sample material, preparation details, and imaging conditions for each of the patterning methods tested

Patterning method	Material	Sample preparation	Imaged resolution
Airbrushed, Surface	ECO	as delivered, fully cured	10μm/pixel
Airbrushed, Internal	Silicone Rubber, GE Silicones	first layer: 24 h at 30°C second layer: 48 h at 30°C	3.0μm/pixel
Nanoparticle, Surface	PDMS	48 hours at 30°	134 nm/pixel
Nanoparticle, Internal	PDMS	first layer–48 hours at 30°C; UV, oxygen plasma treated; second layer–48 hours at 30°C	213 nm/pixel

Fluorescent Nanoparticle DIC Pattern

Surface pattern

For nanoscale measurements, the speckle pattern was created by excitation of fluorescent nanoparticles solution deposited onto the surface of a polymer sample. The nanoparticles were fabricated according to the synthesis procedure outlined by van Blaaderen and Vrij, [14] and Verhaegh and van Blaaderen [15]. The silica nanospheres were labeled with rhodamine B isothiocyanate, with peak excitation frequency of 555 nm. To minimize potential photobleaching upon excitation, the fluorescent dye was incorporated at the nanoparticle core with a subsequently grown outer shell of silica. A mean particle diameter of 140–180 nm was determined by transmission electron microscope (TEM) images such as Fig. 4(a). By dispersing the nanoparticles in ethyl alcohol, a final colloidal suspension with a 3.0% concentration by mass was prepared for the purpose of spin coating.

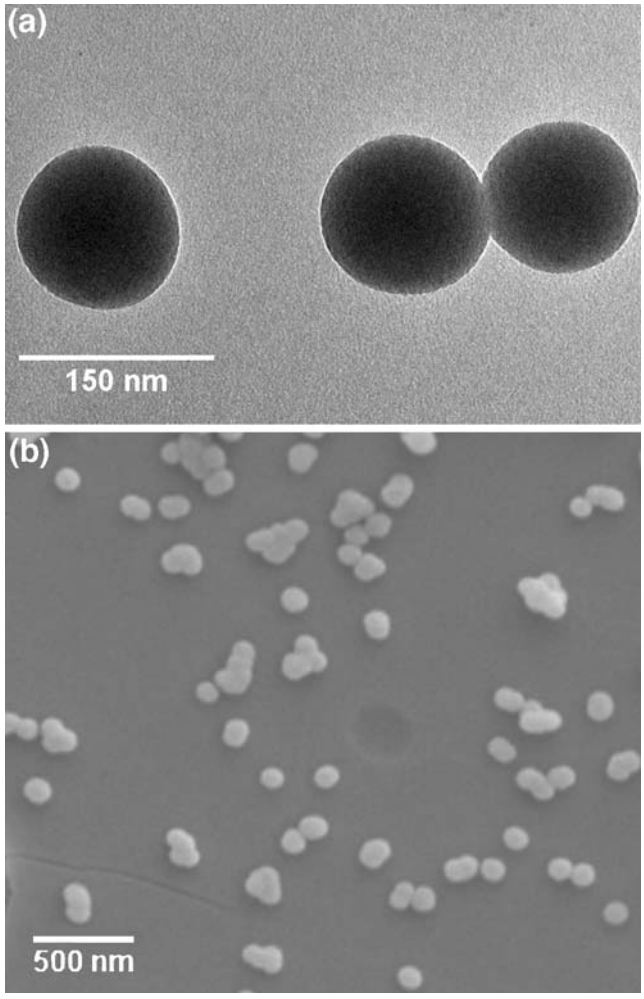

Fig. 4 (**a**) Silica nanoparticles used for internal samples before deposition imaged using a TEM. (**b**) Dispersed nanoparticles on the PDMS sample surface after spincoating under an SEM

Samples were created by casting sheets of Sylgard 184 (Dow Corning) polydimethylsiloxane (PDMS) prepared with a 10:1 ratio of resin to curing agent and a 48 h cure at 30°C. After curing, the sample surface was exposed to a 30 min ultraviolet (UV) box treatment to alter the surface chemistry and enhance adhesion with the silica nanoparticles. A colloidal suspension of fluorescent nanoparticles was then deposited onto the UV treated sample surface at 1,250 rpm, resulting in a monodisperse layer of silica nanoparticles adhered to the PDMS substrate. The SEM micrograph in Fig. 4(b) reveals that the nanoparticles were well adhered and randomly distributed across the sample surface. Upon appropriate light excitation under an optical microscope the nanoparticles fluoresce to a size approximately four to five times their diameter, thus producing a pattern suitable for image correlation, Fig. 1(c).

Internal pattern

Following nearly the same synthesis procedure detailed above, a second batch of fluorescent nanoparticles (ca. 140 nm) was produced. As before, the particles were dispersed in ethanol and diluted to a solution with 3.0% concentration by mass. Samples of PDMS created for internal measurements were built-up using the same two layer approach used for the internally patterned microscale samples. Initially, the bottom half of each sample was poured and fully cured for 48 h at 30°C. Next, the samples were subjected to consecutive treatments in a UV box and an oxygen plasma device (March Plasmod). Immediately following the oxygen plasma treatment, nanoparticles were solution deposited on the surface at 1,250 rpm. Samples were subject to a brief heat treatment (100°C for 30 sec.) to strengthen bonding between the silica nanoparticles and the PDMS surface. The samples were then placed in a mold and an additional layer of PDMS was poured over the nanoparticle-coated surface. After the top layer cured for 48 h at 30°C, the final sample contained an internal layer of fluorescent nanoparticles embedded near the specimen midplane. Upon excitation, the nanoparticles produced a pattern similar to that of the surface coated specimens, Fig. 1(c).

In analogy to the microscale case, an additional set of internally nanoparticle patterned specimens were fabricated which included a sparse concentration of embedded silica glass microspheres with $r = 70 - 80\ \mu$m. The resulting samples had a fluorescent nanoparticle pat-

terned layer just below the embedded silica sphere in the plane $z=-r$, for $z=0$ at the sphere midplane.

Experimental Procedure

Specimen Imaging

Microscale surface patterned samples were imaged using an Olympus SZX-12 stereomicroscope and a 640×480 pixel Sony XC-77 monochrome CCD camera. The resolution of the imaged surface was 10 μm/pixel, producing a total field of view of 6.4×4.8 mm. Internally patterned samples were imaged using a zoom factor of 3.3×, giving a resolution of 3 μm/pixel and a 1.9×1.4 mm field of view. Since both polymers used for microscale tests were completely transparent, a uniformly white background was positioned behind the specimens to provide contrast with the black paint speckles during testing. Nanoparticle coated specimens were imaged under a Leica DM-R fluorescent microscope (with Hg lamp excitation source) using a QImaging Retiga monochrome CCD camera with 1,280×1,024 pixel resolution. For surface coated specimens, a 50× long working distance objective lens with no camera relay lens was used, giving an image resolution of 134 nm/pixel and a total field of view of roughly 170×140 μm. Internally patterned samples were imaged slightly differently by adding a 0.63× relay lens. This modified imaging set-up produced a resolution of 213 nm/pixel, with a total field of view roughly 270×220 μm. Microsphere embedded samples were imaged at a pixel resolution of 533 nm/pixel, which gives a pattern acceptable for correlation while allowing for a greater field of view. For all fluorescent nanoparticle patterns, the background was dark and the spheres appeared white upon excitation when viewed with a black and white camera.

Imaging conditions for the fluorescent nanoparticle coated specimens were adjusted to minimize any photobleaching of the fluorescent dye. If photobleaching induced variations in the emitted light intensity created significant changes in the imaged pattern, poor correlation and erroneous displacement measurements were observed. As expected, the intensity of the excitation light source significantly affected the rate of bleaching. For the surface patterned samples, the effect of excitation intensity on nanoparticle photobleaching was investigated by taking a series of time-lapse images of undeformed patterned samples under different lighting conditions. As shown in Fig. 5, light sources near the dye excitation frequency resulted in significant declines in the measured mean image intensity (labeled "max" and "low"). Greater stability in pixel intensity was obtained by lowering the intensity of the excitation light source and using auxiliary light sources at frequencies different from the peak excitation frequency of the fluorescent nanoparticles.

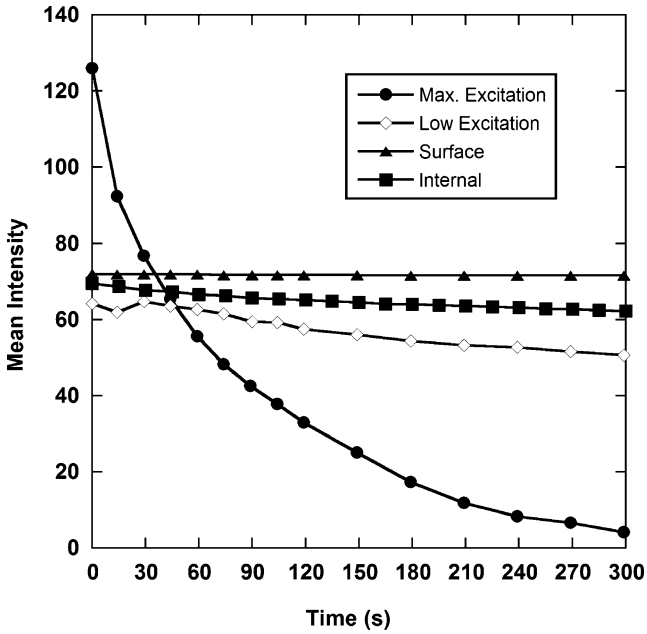

Fig. 5 Mean intensity of nanoparticle patterned samples over time under excitation using a variety of illumination conditions

For the internally embedded nanoparticle samples, a longer exposure time and less auxiliary light were necessary to produce images with the appropriate pattern contrast. These modifications did result in a slight increase in photobleaching rate compared to the surface patterned specimens. However, correlations performed on time-lapse images of undeformed specimens showed that photobleaching had no noticeable effect on the pattern quality or DIC measurements for the time scales associated with the testing in this work.

Baseline Tests

Noise levels associated with room vibrations, temperature fluctuations, etc., were determined by performing baseline tests in which no deformations was applied. Tests on both the surface and internally patterned microscale airbrushed samples showed an average random noise level of ±0.5 μm (0.05 pixels). Conversely, baseline tests performed on the samples surface coated with nanoparticles displayed an average ±7 nm (0.05 pixels) measured noise level in either direction, while the samples internally patterned with nanoparticles had an average of ±18 nm (0.08 pixels)

measured noise. Additionally, image variations introduced by refocusing on the patterned plane were measured by comparing images of an undeformed pattern taken before and after refocusing on the same plane. For the nanoparticle coated samples, the pattern layer provided a particularly distinct focal plane which helped ensure that the same image plane was found. The variations in displacement upon refocusing were indistinguishable from the baseline noise level for each pattern type.

Rigid Body Translations

For rigid body tests, samples were attached to a calibrated actuator stage and translated uniformly in one direction. For the airbrushed samples, rigid body translations over the range of 10 to 100 μm were applied using a computer-controlled servo motor with sub-micron precision (Polytec-PI, Model M-224.50) to drive an actuator stage. Translations for the nanoparticle samples were provided over a range from 10 to 100 nm by applying a series of DC voltages to a piezostack actuator stage (Thor Labs, Model PE4).

Tensile Tests

Tensile testing of both the microscale airbrushed and the nanoparticle coated specimens was performed using a DC-mike actuator (Polytec-PI, Model M-224.50) connected to a tensile grip. The other tensile grip was rigidly mounted to a support frame and did not move. Care was taken during the grip alignment to ensure that imaged plane of the sample remained flat for the course of the experiment. Samples for all tests were cut from patterned full sheets of the elastomer material to final dimensions of 8.0 mm wide by 30 mm long. The ends of the samples were fixed in the tensile grips, such that the initial distance between the grips was approximately 20 mm. All samples were then loaded quasi-statically and imaged under an optical microscope, with continuous image acquisition of the patterned area throughout the duration of the test. Microscale airbrush and nanoparticle coated samples were tested at extensional rates of 1.0 and 0.1 μm/sec, respectively. Samples containing just the patterned layer were tested over a range of strains to determine system resolution capabilities, while a constant 3.5% strain was applied to specimens with embedded glass microspheres. Results of the tensile tests are provided in "Results".

Results

Rigid Body Translations

The displacements measured by DIC are compared with the applied translations in Fig. 6(a) for both surface and internal airbrush patterned samples. For each translation, the average displacement was calculated from the entire DIC produced vector field of correlation points. The DIC measured displacements corresponded well with the translations applied from 100 down to 1.0 μm for the surface patterned samples. Beyond this lower limit, there were marked increases in the standard deviation of measured displacement, as well as more variability in DIC vector field directionality. These limitations are expected as the size of the applied translations approaches the baseline noise level.

The average DIC measured displacements for the internally patterned microscale specimens were con-

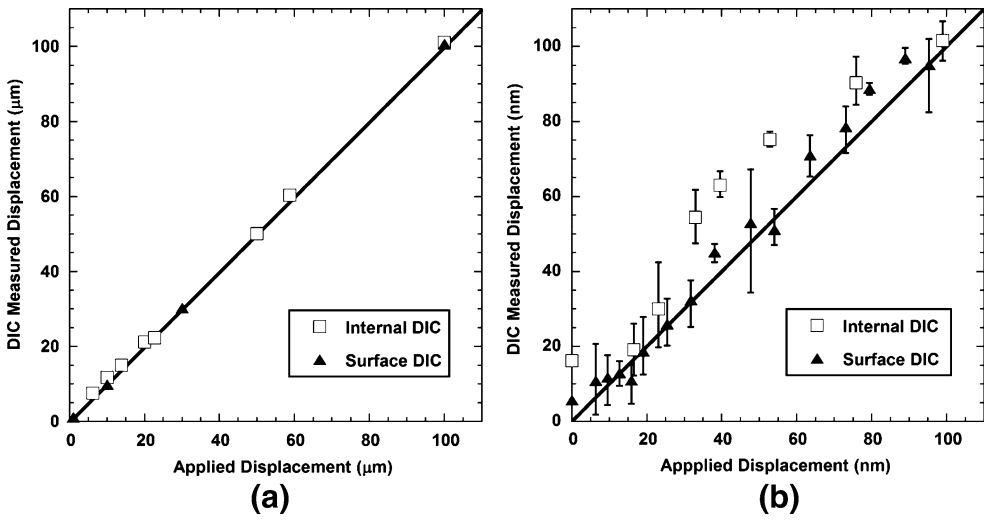

Fig. 6 Comparison of internal and surface DIC measurements of rigid body translations versus the applied translation for (**a**) paint speckle pattern, and (**b**) nanoparticle speckle pattern

sistent with the applied translations across most of the range tested. However, the standard deviation of the displacement measurement across the DIC generated vector field was significant (greater than 5%) for applied translations below 20 μm. The increased error may be due in part to the change in index of refraction in the optical path. Surface patterned samples are imaged through air (n=1.003) only, while internally patterned samples are imaged through air and 1.5 mm of GE Silicones RTV-615 (n=1.406) or PMDS (n=1.41).

For the nanoparticle patterned samples, the average displacement was once again calculated from the DIC generated vector field and plotted against the applied translation, Fig. 6(b)—note the difference in scale from Fig. 6(a). The error bars reflect the scatter observed in this measurement over three separate tests. For the surface patterned nanoparticle samples, DIC measurements of translations in the range from 20–100 nm produced uniform vector fields with minimal variation in vector magnitude or direction and that were consistently within 15–20 nm of the applied translation. As the applied translations were reduced below 20 nm, there was a significant increase in the DIC vector field directionality scatter. This same increase in variability was observed to occur for applied translations below 40 nm for the internally patterned nanoparticle samples, Fig. 7. The lower limit of measurable translations in this case corresponds to approximately one-sixth to one-fifth of a pixel, compared with the previously mentioned one-tenth to one-eighth pixel.

The lower limit for the accuracy in DIC measurements of nanoscale displacements is directly related to the background noise level of the imaging set-up. Major contributors to the noise include thermal drift and set-up vibrations. The baseline tests made no separation of these contributions, and simply characterized the overall noise magnitude for each set of patterns and imaging conditions. In general, the DIC displacement resolution limit for the internally patterned samples was slightly worse than the surface patterned samples, which may be attributed to the change in index of refraction in the optical path (air versus air plus 1.5 mm of PDMS). Additionally, the internal nanoparticle patterned samples showed a disproportionately higher noise level in the baseline tests compared to that measured for the surface nanoparticle patterned samples. This result was expected in accordance with the extended exposure time necessary for imaging the internally embedded fluorescent nanoparticle pattern (10 sec, as opposed to the 300 ms exposure for the surface nanosphere patterned specimens), which makes those measurements more susceptible to random noise disturbances. Despite the reduced resolution limit for the internal nanoparticle patterned samples, the DIC measured translations from 40–100 nm agreed well with the applied translations, consistently falling within 35 nm.

Tensile Tests on Patterned Uniform Samples

For all samples loaded in uniaxial tension, DIC measured contours of constant displacement were used to calculate the average strain across the field of view. The locally measured strain was then used to calculate the expected far-field displacement based on the initial gage length and the assumption of uniform sample deformation. The results for the microscale airbrushed samples, Fig. 8(a), and the nanoparticle coated specimens, Fig. 8(b), are plotted against the applied far-field displacement.

For both the internal and surface airbrush patterned samples, local strains calculated from DIC contours of

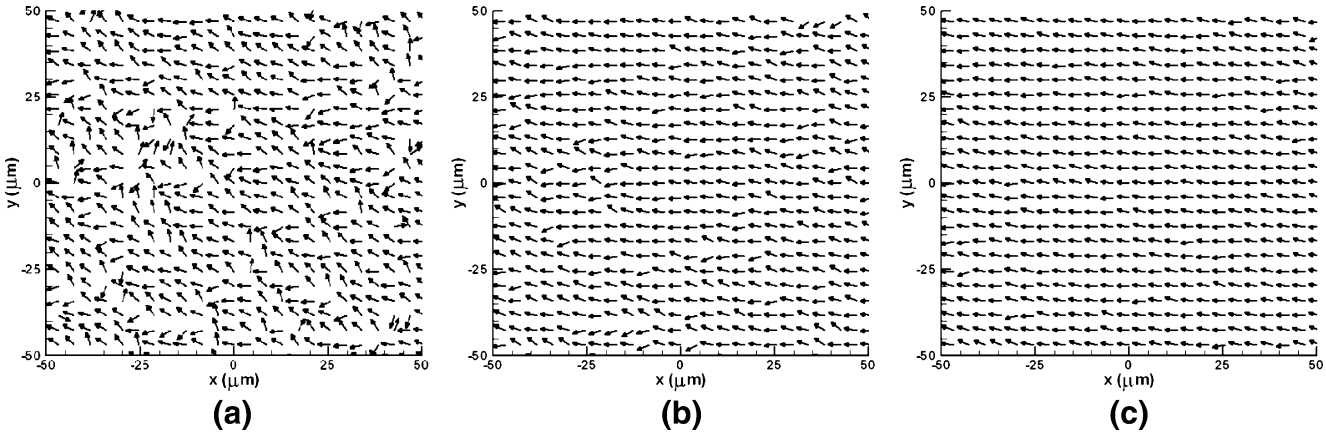

Fig. 7 Vector plots of DIC measured translations on an internally nanoparticle patterned sample, where the applied displacement in the "x" direction is 16 nm (**a**), 40 nm (**b**), and 76 nm (**c**)

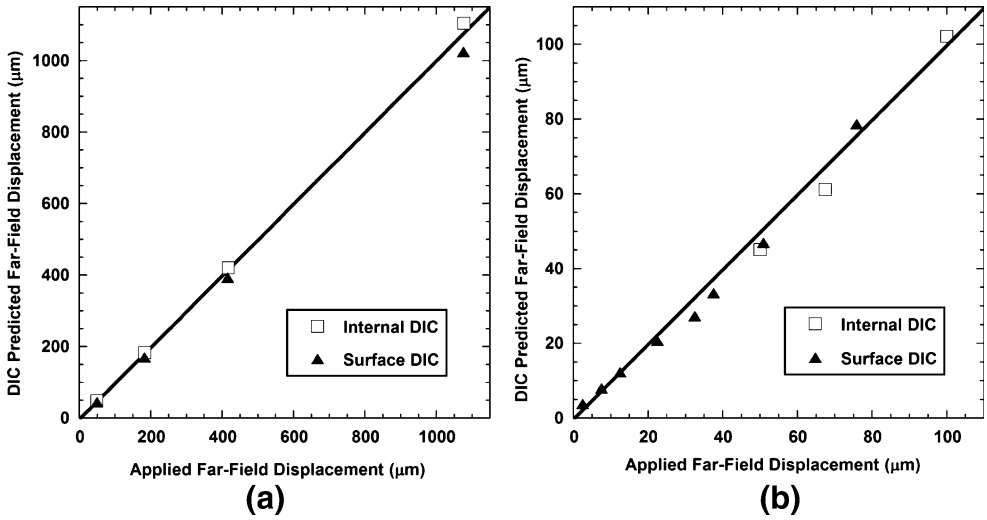

Fig. 8 Comparison of far-field tensile displacements, calculated from local DIC measurements on both internal and surface specimens, against the applied far-field displacement for (**a**) paint speckle patterned, and (**b**) nanoparticle coated samples

constant displacement were close to the actual applied far-field strains. In each case, the most deviation came at the highest applied strain level. Possible reasons for this discrepancy include issues associated with the sample grips (slipping, etc.) and the potential for a non-uniform strain fields due to sample barreling. Also, the largest applied deformations are getting away from the small strain regime to which this DIC method should be confined. In both types of micro-scale airbrush patterned samples, the closest distinguishable contours of constant displacement were typically 1–5 μm.

DIC results from tensile tests on the surface coated nanoparticle samples revealed contours of constant displacement differing by only 20 nm, consistent with the measurement resolution limit found for rigid body translation tests. For the internally patterned samples, the DIC contour line threshold shown in Fig. 9 was roughly 35 nm. While the DIC results from the internally patterned samples had more noise in the contour lines for the smallest applied strain levels, far-field applied displacements were accurately measured.

Tensile Tests on Embedded Inclusion Samples

Airbrush samples with a dilute concentration of internally embedded silica microspheres, with the same dimensions as Fig. 3(b), were loaded in uniaxial tension at a strain level of 3.5%. With the large depth of field for the low magnification used in imaging the internal airbrushed pattern, the location of a single microsphere could easily be determined when focusing

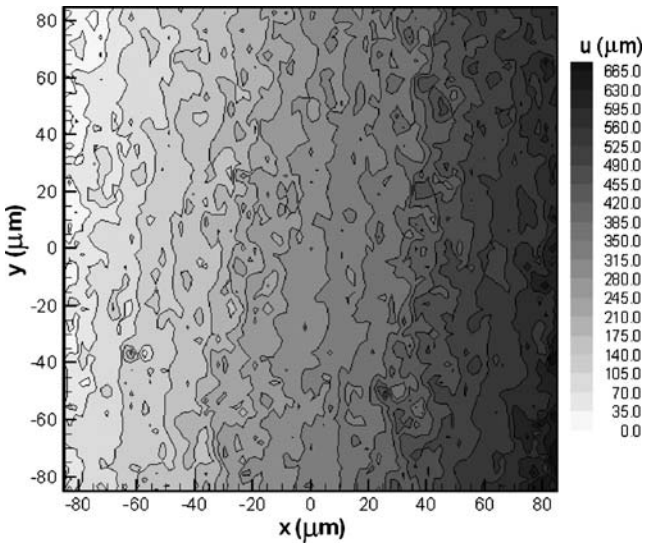

Fig. 9 Contours of constant displacement for an internally embedded layer of fluorescent nanoparticles in a PDMS sample loaded in tension at an applied strain level of 0.37%

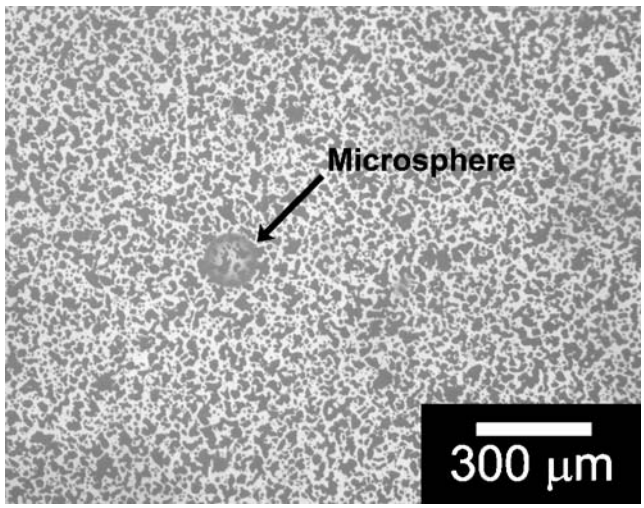

Fig. 10 Rigid silica microsphere internally embedded at the midplane of a PDMS sample. An airbrush patterned layer, located at the bottom of the sphere, is used to determine the deformation field of that plane for an applied uniaxial tension

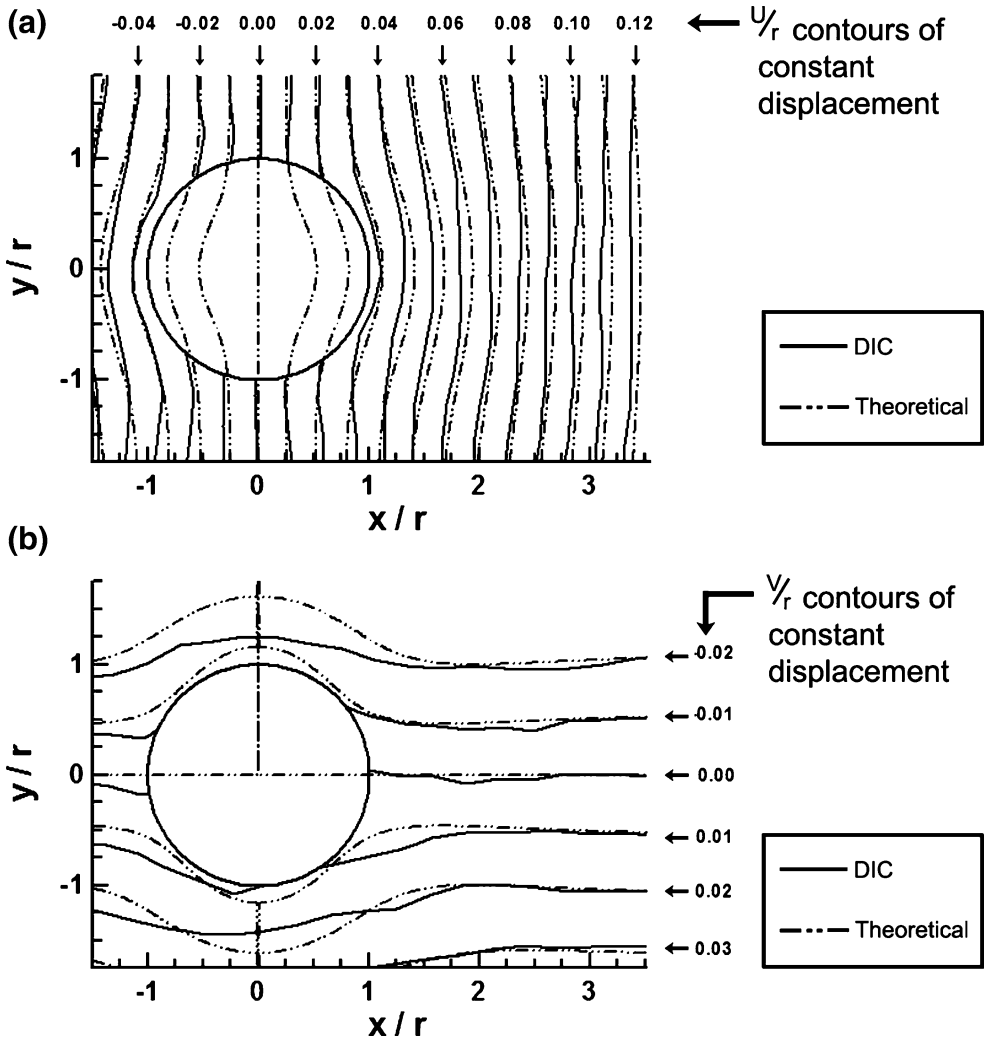

Fig. 11 Deformation fields showing "u" (**a**) and "v" (**b**) displacements near a silica microsphere (radius r=73 μm) internally embedded in a PDMS sample loaded in uniaxial tension (3.5% strain). For each displacement component, experimental DIC measurements for the airbrushed pattern are compared with the predicted analytical solution of a rigid spherical inclusion proposed by Goodier [16] for the plane $z=r$ (where the z=0 for the sphere midplane)

on the patterned layer below, as shown in Fig. 10. Experimental DIC measurements of the displacement field surrounding the microsphere were compared to the theoretically predicted field near a rigid inclusion (the $z=-r$ plane, for z=0 at the sphere midplane) in an elastic infinite medium under a remote tensile stress as determined by Goodier [16]. The sparseness of the silica microsphere inclusions is such that we can effectively consider the microsphere isolated and therefore make valid comparisons with the Goodier solution for a rigid sphere in an infinite elastic space. Furthermore, because of the large elastic property mismatch between PDMS and silica glass, the microsphere is considered rigid. Finally, at the small strains applied in the experiments the PDMS should behave in a linear elastic fashion. For the microscale pattern

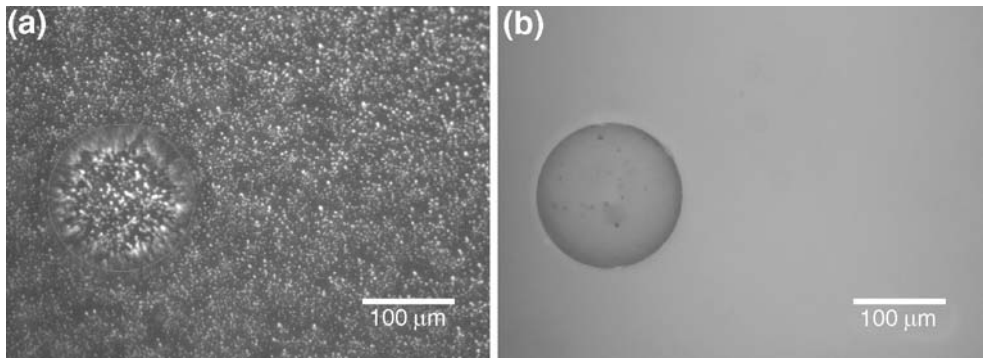

Fig. 12 Image focused on a fluorescently excited nanoparticle patterned layer, (**a**) located just below a rigid silica microsphere embedded within a PDMS sample. The exact location of the microsphere is determined by focusing at the sphere midplane under normal lighting conditions (**b**)

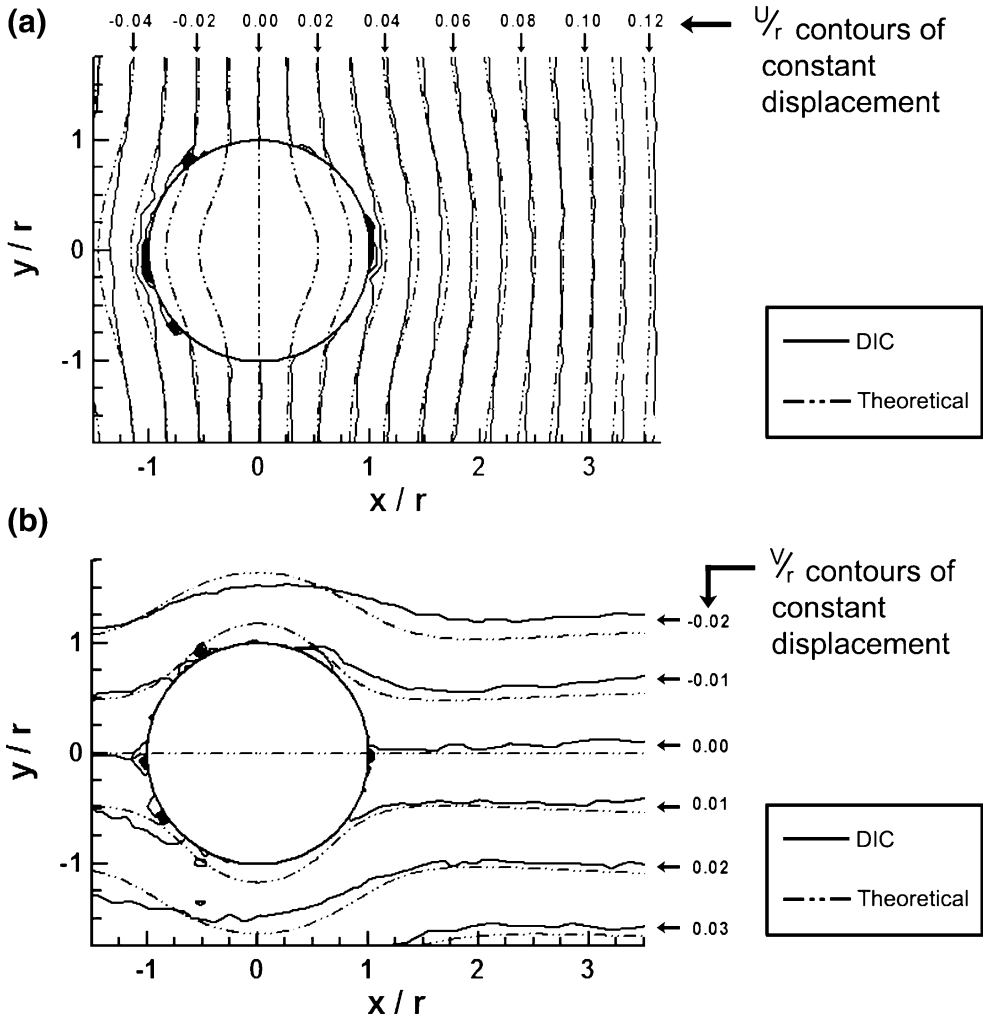

Fig. 13 Deformation fields showing "*u*" (**a**) and "*v*" (**b**) displacements near a silica microsphere (radius *r*=78 μm) internally embedded in a PDMS loaded in uniaxial tension (3.5% strain). Experimental results via DIC measurements on the internal nanoparticle pattern are shown with the predicted analytical solution [16] for the plane *z*=*r* (where the *z*=0 for the sphere midplane)

case, contours of "*u*" displacement in the loading direction, are shown in Fig. 11(a). The far-field strain was in good agreement to the actual applied strain. Closer to the sphere, however, the DIC measurements showed increased variability and deviations from the analytical solution. The difference in the local theoretical and experimental displacement fields was even greater for the contours of "*v*" displacement, shown in Fig. 11(b). The increased variability is expected for the much smaller deformations measured in this direction.

A sample with a similarly sized silica microsphere embedded just above an internal fluorescent nanoparticle pattern layer [Fig. 12(a) and (b)] was also loaded to a far-field strain level of 3.5%. The DIC "*u*" contours of displacement [Fig. 13(a)] showed much less variation from the theoretical predictions than the airbrush pattern, especially very close to the microsphere. The "*v*" contours found from DIC measurements [Fig. 13(b)] were much closer to the theoretical field for the nanoparticle pattern than those found for its counterpart internal airbrush patterned sample under the same loading. The airbrush pattern was not refined enough to discern the intricacies of the displacement field on this size-scale. On the other hand, the nanoparticle speckle pattern enables measurement of an accurate deformation field across a highly localized field of view through higher magnification and spatial resolution. Optimization of the imaging parameters with this method should allow for deformation field measurements surrounding nanoscale inclusions, while the extension of this technique to capture full-field deformations on an internal sample plane lends itself to possible 3D volumetric measurements similar those made in confocal techniques.

Conclusion

We have demonstrated the feasibility of the DIC technique to image planar deformations at both the

microscale and the nanoscale using a simple set-up based on optical microscopy. Successful application of DIC at the different length scales relied on the ability to generate a speckle pattern at the scale under consideration. The microscale pattern was generated using a fine point airbrush to deposit paint on the specimen surface. The nanoscale pattern was produced by solution deposition of a monodisperse layer of fluorescent rhodamine dye infused silica nanoparticles (140–180 nm in diameter) on the specimen surface. When excited appropriately, the nanoparticles fluoresced to a size scale several times their diameter and generated a pattern that can be imaged in an optical microscope and used for DIC. The use of fluorescent nanoparticles was a significant development in that the particles allow for nanoscale displacement detection while minimally disturbing the structure under interrogation. Rigid body translation and uniaxial tensile testing were used to investigate the lower limits of measurement accuracy at each length scale. Suitable patterns were generated for testing at the microscale with measurement resolution of 1 μm, and the nanoscale with a resolution of resolution of 17 nm. Finally, the technique was extended to making similar internal microscale and nanoscale measurements in a deforming transparent polymer with an embedded speckle pattern at its midplane. A comparison of DIC measured deformation fields surrounding a micron-scale rigid inclusion for both nanoparticle and airbrush internally patterned samples loaded in uniaxial tension provided an example of the relative accuracy and operating size-scale for the two patterning methods.

Acknowledgments The authors would like to acknowledge the support of the AFOSR (MURI Award No. F49550-05-1-0346), the NSF (grant CMS 00-8206) and the U.S. Department of Enegy, Division of Materials Sciences (Award No. DEFG02-91ER45439), through the Federick Seitz Materials Research Laboratory at the University of Illinois at Urbana–Champaign. Additionally, R.G.S. acknowledges fellowship support from the Fannie and John Hertz Foundation.

References

1. Nalla RK, Kinney JH, Ritchie RO (2003) Mechanistic fracture criteria for the failure of human cortical bone. Nat Mater 2(3):164–168.
2. Peters WH, Ranson WF (1982) Digital imaging techniques in experimental stress analysis. Opt Eng 21(3):427–431.
3. Sutton MA, Wolters WJ, Peters WH, Ranson WF, McNeill SR (1983) Determination of displacements using an improved digital image correlation method. Image Vis Comput 1(3):133–139.
4. Peters WH, Ranson WF, Sutton MA, Chu TC, Anderson J (1983) Application of digital correlation methods to rigid body mechanics. Opt Eng 22(6):738–742.
5. Chu TC, Ranson WF, Sutton MA, Peters WH (1985) Applications of digital-image-correlation techniques to experimental mechanics. Exp Mech 25(3):232–244.
6. Chasiotis I, Knauss WG (2002) A new microtensile tester for the study of MEMS materials with the aid of atomic force microscopy. Exp Mech 42(1):51–57.
7. Schreier HW, Braasch JR, Sutton MA (2000) Systematic errors in digital image correlation caused by intensity interpolation. Opt Eng 39(11):2915–2921.
8. Gonzalez J, Knauss WG (1998) Strain inhomogeneity and discontinuous crack growth in a particulate composite. J Mech Phys Solids 46(10):1981–1995.
9. Abanto-Bueno J, Lambros J (2005) Experimental determination of cohesive failure properties of a photodegradable copolymer. Exp Mech 45(2):144–152.
10. Vendroux G, Schmidt N, Knauss WG (1998) Submicron deformation field measurements: part 3. demonstration of deformation determinations. Exp Mech 38(3):154–160.
11. Abanto-Bueno J, Lambros J (2004) Mechanical and fracture behavior of an artificially ultraviolet-irradiated poly(ethylene-carbon monoxide) copolymer. J Appl Polym Sci 92(1):139–148.
12. Berfield TA, Patel JK, Shimmin RG, Braun PV, Lambros J, Sottos NR (2006) Fluorescent image correlation for nanoscale deformation measurements. Small 2(5):631.
13. Patel JK (2003) Digital image correlation for microscale and nanoscale deformation measurement. M.S. Thesis, University of Illinois at Urbana–Champaign.
14. van Blaaderen A, Vrij A (1992) Synthesis and characterization of colloidal dispersions of fluorescent, monodisperse silica spheres. Langmuir 8(12):2921–2931.
15. Verhaegh NAM, van Blaaderen A (1994) Dispersions of rhodamine-labeled silica spheres. synthesis, characterization, and fluorescence confocal scanning laser microscopy. Langmuir 10(5):1427–1438.
16. Goodier JN (1933) Concentration of stress around spherical and cylindrical inclusions and flaws. Appl Mech 1(2):39.